

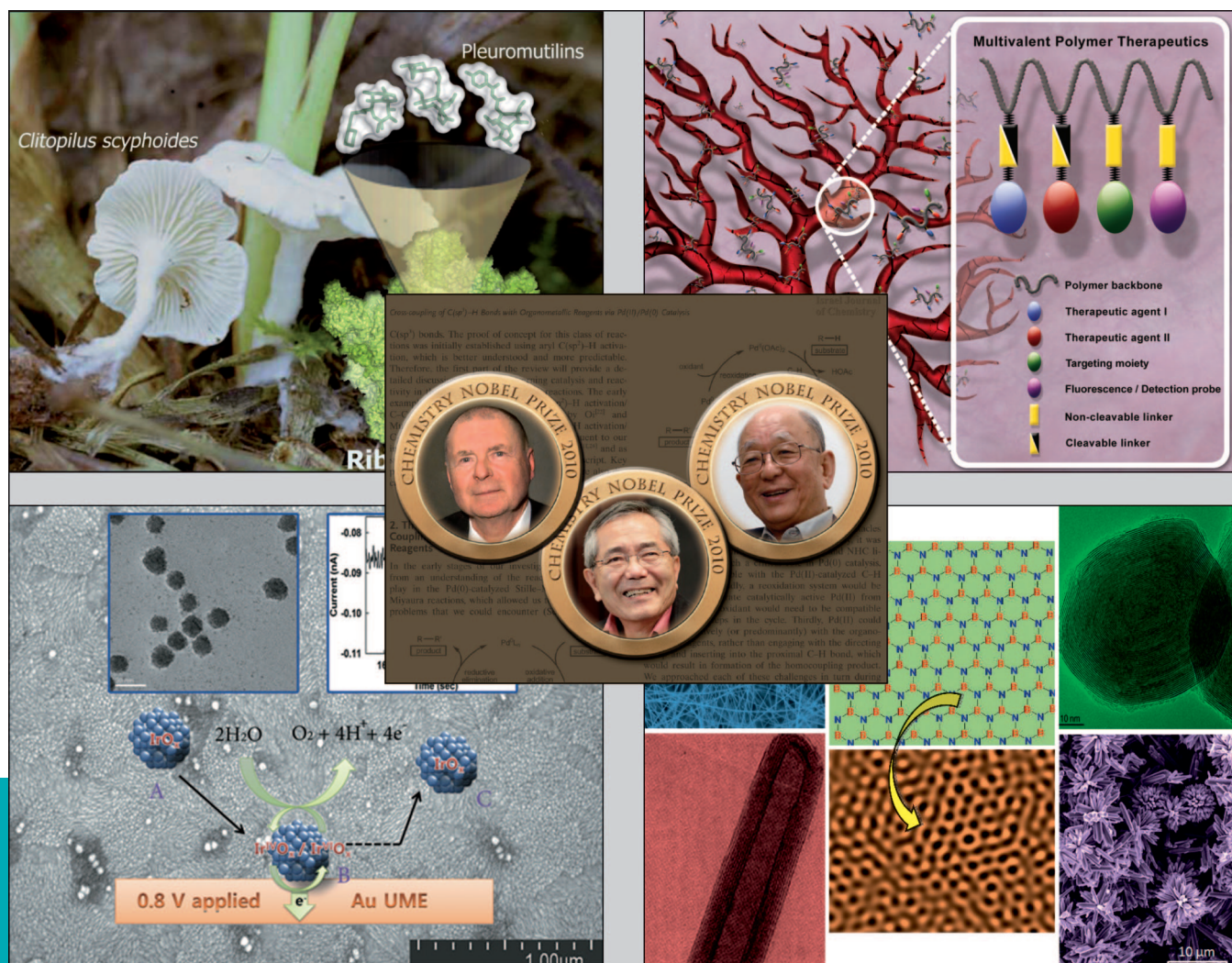
# Israel Journal of Chemistry



Official Journal of the Israel Chemical Society

## REPRINT

[www.ijc.wiley-vch.de](http://www.ijc.wiley-vch.de)



WILEY-VCH

# Separation of Xenon and Krypton in the Metal–Organic Frameworks $M_2(m\text{-dobdc})$ ( $M = \text{Co}, \text{Ni}$ )

Matthew T. Kapelewski,<sup>[a]</sup> Julia Oktawiec,<sup>[a]</sup> Tomče Runčevski,<sup>[a]</sup> Miguel I. Gonzalez,<sup>[a]</sup> and Jeffrey R. Long<sup>\*,[a, b, c]</sup>

**Abstract:** The separation of Xe and Kr from air is challenging owing both to the very low atmospheric concentrations of these gases and the need for their distillation at cryogenic temperatures. Alternatively, separation processes based on adsorption could provide a less energy-intensive route to the isolation of these gases. Here, we demonstrate that the metal–organic frameworks  $M_2(m\text{-dobdc})$  ( $M = \text{Co}, \text{Ni}$ ;  $m\text{-dobdc}^{4-} = 4,6\text{-dioxido-1,3-benzenedicarboxylate}$ ) effectively separate Xe and Kr at ambient temperatures based on the different adsorption enthalpies of each gas at the coordinatively-unsaturated  $M^{2+}$  sites in each material. *In situ* Xe- and Kr-dosed powder X-ray diffraction studies further reveal key

differences in the binding of Xe and Kr within the materials. In particular, while both gases adsorb near the framework open metal sites at 200 K, much higher Xe occupancies are observed at these sites relative to Kr, corroborating a stronger interaction of the polarizing  $M^{2+}$  cations with Xe. Further, while krypton is only found located above the open metal sites, two additional adsorption sites are observed for xenon, correlating with the stronger adsorption of Xe over Kr in these materials. These results suggest the possible utility of employing  $M_2(m\text{-dobdc})$  materials in the adsorptive separation of Xe and Kr.

**Keywords:** Metal-Organic Frameworks · Gas separations · Porous Materials · Open Metal Coordination Sites

## 1. Introduction

The noble gases xenon and krypton are used in a variety of applications, such as photography lighting, lasers, and as high-purity samples in scientific laboratories. Xenon is also used as a general anesthetic and space propellant,<sup>[1]</sup> while Kr is used as an MRI contrast agent.<sup>[2]</sup> However, obtaining pure Xe and Kr requires distillation from air, which is energetically and financially costly due to their very low atmospheric concentrations – 1.14 and 0.086 ppm for Kr and Xe, respectively.<sup>[3]</sup> Currently, pure Xe and Kr are obtained by first isolating a byproduct stream (composed of 80% Kr and 20% Xe) from the cryogenic distillation of air, compressing this stream to 200 bar, and sending it to a plant where it is separated into the pure components through a second cryogenic distillation process.<sup>[1]</sup> The significant energetic cost of this process further contributes to the high prices of these gases – most notably Xe, which costs about \$5000/kg.<sup>[4]</sup>

Implementation of an adsorption-based process for a Xe/Kr separation could potentially lower the overall production costs for these noble gases, by enabling their separation at near ambient temperatures. Toward this end, various materials – including activated carbons,<sup>[5]</sup> zeolites,<sup>[5b,6]</sup> porous organic cages,<sup>[4]</sup> and metal-organic frameworks (MOFs)<sup>[7,8]</sup> – have been explored for their ability to separate mixtures of Xe and Kr. Metal-organic frameworks exhibit particular promise in this regard, as their highly tunable structures allow for the design of pore environments that facilitate selective binding. In particular, various frameworks with coordinatively-unsaturated metal centers exhibit some of the highest Xe/Kr selectivities,<sup>[9]</sup> as adsorption of these gases is exclusively


dependent on the polarization of the electron cloud surrounding each atom, and the positively charged metal cations are able to more strongly polarize Xe over Kr. Members of the  $M_2(\text{dobdc})$  family of frameworks (also known as M-MOF-74, CPO-27-M, and  $M_2(\text{dhtp})$ ;  $M = \text{Mg}, \text{Mn}, \text{Fe}, \text{Co}, \text{Ni}, \text{Cu}, \text{Zn}, \text{Cd}$ ;  $\text{dobdc}^{4-} = 2,5\text{-dioxido-1,4-benzenedicarboxylate}$ )<sup>[10]</sup> have received particular focus in this regard. For example, selective adsorption of Xe out of a mixture of Kr and other gases resulting from nuclear fuel reprocessing was demonstrated in  $\text{Ni}_2(\text{dobdc})$ .<sup>[11]</sup> Subsequent work has shown that  $\text{Co}_2(\text{dobdc})$  is capable of the dynamic separation of a Xe/Kr mixture,<sup>[12]</sup> and a detailed study of Xe and Kr adsorption sites and pore filling in  $M_2(\text{dobdc})$  ( $M = \text{Mg}, \text{Ni}$ ) was carried out using *in situ* powder X-ray diffraction.<sup>[9c]</sup> Computational research has also provided insight into the effect of different metal centers on the adsorption of Xe and Kr at the open metal sites.<sup>[13]</sup>

Considering the demonstrated utility of  $M_2(\text{dobdc})$  materials in separating Xe and Kr, we sought to investigate the

[a] M. T. Kapelewski, J. Oktawiec, T. Runčevski, M. I. Gonzalez, J. R. Long  
Department of Chemistry, University of California, Berkeley, Berkeley, California 94720, USA

[b] J. R. Long  
Department of Chemical Engineering, University of California, Berkeley, Berkeley, California 94720, USA

[c] J. R. Long  
Materials Sciences Division, Lawrence Berkeley National Laboratory, Berkeley, California 94720, USA

 Supporting information for this article is available on the WWW under <https://doi.org/10.1002/ijch.201800117>

related metal–organic frameworks  $M_2(m\text{-dobdc})$  ( $M=\text{Mg, Mn, Fe, Co, Ni}$ ;  $m\text{-dobdc}^{4-}$  = 4,6-dioxido-1,3-benzenedicarboxylate)<sup>[14]</sup> for this application. These frameworks are structural isomers of  $M_2(\text{dobdc})$  and have been studied extensively for  $\text{H}_2$  adsorption. The  $M_2(m\text{-dobdc})$  frameworks notably display larger hydrogen binding enthalpies than their  $M_2(\text{dobdc})$  counterparts, due to increased positive charge at their open metal sites that results from the altered linker geometry. This increased charge density induces greater polarization of the  $\text{H}_2$  electron cloud, resulting in the stronger binding at the open metal centers in these frameworks relative to  $M_2(\text{dobdc})$ . The low-cost of the  $m\text{-dobdc}^{4-}$  ligand is an added advantage that lends itself to the economical large-scale synthesis of  $M_2(m\text{-dobdc})$  as an adsorbent for industrial separations.<sup>15</sup>

Herein, we detail the investigation of  $\text{Co}_2(m\text{-dobdc})$  and  $\text{Ni}_2(m\text{-dobdc})$  as selective adsorbents for Xe over Kr. Selectivities predicted by ideal adsorbed solution theory and calculated differential enthalpies of adsorption – based on fits to single-component Xe and Kr adsorption isotherms – confirm that  $\text{Co}_2(m\text{-dobdc})$  and  $\text{Ni}_2(m\text{-dobdc})$  more strongly adsorb xenon relative to krypton, consistent with the greater polarizability of xenon. Additionally, *in situ* gas-dosing powder X-ray diffraction experiments reveal clear differences in the xenon and krypton adsorption sites and occupancies, corresponding well with the results from the gas adsorption experiments.

## 2. Experimental Section

**Synthesis of  $M_2(m\text{-dobdc})$ .**  $M_2(m\text{-dobdc})$  ( $M=\text{Co, Ni}$ ) were synthesized using a previously reported procedure.<sup>[16]</sup>

**Gas Adsorption Measurements.** Gas adsorption isotherms were measured on either a Micromeritics ASAP2020 HD or 3Flex instrument. Samples were first activated at 120 °C under vacuum in a Schlenk flask and then transferred to a preweighed glass sample tube in a dry box under an  $\text{N}_2$  atmosphere and capped with a Micromeritics Transeal. The samples were further activated in the sample tube on the degas manifold of the ASAP2020 HD instrument at 180 °C under high vacuum for at least 24 h. The sample tube was then weighed to determine the mass of the degassed sample, typically 100–500 mg. The tube was then transferred to the analysis port of the instrument. All measurements used ultra-high purity (99.999%)  $\text{N}_2$ , He, Xe, and Kr as well as oil-free vacuum pumps and pressure regulators. Xenon and Krypton isotherms were measured at 25, 35, and 45 °C using a Julabo circulating water bath for temperature control. Samples were heated to 180 °C under vacuum after the He free space measurement was completed in order to ensure full evacuation of all He in the sample.

**Isotherm Fitting, Binding Enthalpy Calculations, and Ideal Adsorbed Solution Theory Selectivity Calculations.** To ensure high quality fits, the isotherms at all three temperatures for each gas were fit simultaneously using a tri-site Langmuir equation according to the equation below:

$$n = \frac{q_{\text{sat,A}}b_{\text{AP}}}{1+b_{\text{AP}}} + \frac{q_{\text{sat,B}}b_{\text{BP}}}{1+b_{\text{BP}}} + \frac{q_{\text{sat,C}}b_{\text{CP}}}{1+b_{\text{CP}}}$$

in which  $n$  is the amount adsorbed (in mmol/g),  $q$  is the saturation loading at site A, B, or C (in mmol/g),  $b$  is the Langmuir parameter at site A, B, or C (in  $\text{bar}^{-1}$ ), and  $p$  is the pressure (in bar). The value for  $b$  was calculated using the equation below:

$$b = b_0 e^{-\frac{E}{RT}}$$

From the Langmuir equation fits to the isotherm data, data points at equivalent loadings for each temperature were interpolated using Wolfram Mathematica 11.0. These points were then used with the Clausius–Clapeyron relation to calculate isosteric heats of adsorption for each gas, in each material, according to the equation:

$$h = -R \frac{d(\ln P)}{d\left(\frac{1}{T}\right)}$$

in which  $h$  is the calculated isosteric heat of adsorption,  $R$  is the ideal gas constant,  $P$  is the pressure at a given loading, and  $T$  is the temperature at which the isotherm data was collected (298.15, 308.15, or 318.15 K).

Ideal Adsorbed Solution Theory (IAST) was used to determine selectivities for binding Xe over Kr, first by numerically solving for the spreading pressure and then identifying the composition of the adsorbed phase at a given gas phase composition. The selectivity is given by the following equation:

$$S = \frac{x_{\text{Xe}}/x_{\text{Kr}}}{y_{\text{Xe}}/y_{\text{Kr}}}$$

in which  $S$  is the selectivity,  $x$  is the mole fraction in the adsorbed phase, and  $y$  is the mole fraction in the gas phase.

***In situ* Powder X-ray Diffraction.** High-resolution powder X-ray diffraction patterns were collected at Beamline 17-BM-B at the Advanced Photon Source of Argonne National Laboratory, with an average wavelength of 0.72768 Å. Scattered intensity was recorded by a PerkinElmer a-Si Flat Panel detector. Prior to measurement, samples were packed in borosilicate glass capillaries of 1.0 mm diameter under a  $\text{N}_2$  atmosphere. Each capillary was attached to a custom-designed gas-dosing cell equipped with a gas valve, which was then mounted onto the goniometer head and connected to a gas-dosing manifold for *in situ* diffraction measurements. Sample temperature was controlled by an Oxford CryoSystems Cryostream 800. Diffraction patterns were collected at room temperature under dynamic vacuum to confirm complete desolvation of the framework. The gas-dosing manifold was then used to dose the frameworks with low pressures (70–120 mbar) of Kr or Xe gas at room temperature. After reaching equilibrium (typically less than fifteen minutes), as

confirmed by diffraction patterns, the samples were slowly cooled to 200 K. Rietveld refinement was performed on powder X-ray diffraction data collected at 250 and 200 K. Analysis of all diffraction data is provided in the Supporting Information.

**In situ Single-Crystal X-ray Diffraction.** Single-crystal X-ray diffraction measurements of  $\text{Co}_2(m\text{-dobdc})$  were performed on crystals in xenon-dosed capillaries. A methanol-solvated crystal of  $\text{Co}_2(m\text{-dobdc})$  was first mounted onto a borosilicate glass fiber using a minimal amount of epoxy, ensuring accessibility of the crystal pores. The glass fiber was then inserted into a 1.0 mm borosilicate glass capillary, which was connected to a capillary-dosing assembly attached to a port on a Micromeritics ASAP2020 HD instrument. The sample was evacuated under reduced pressure at 180 °C for 24 h to remove all solvent molecules within the crystal. The capillary was then dosed with 400 mbar of xenon, and finally flame-sealed with a  $\text{CH}_4/\text{O}_2$  torch.

X-ray diffraction data for  $\text{Co}_2(m\text{-dobdc})(\text{H}_2\text{O})_{0.9}0.7\text{Xe}$  were collected at Beamline 11.3.1 at the Advanced Light Source, Lawrence Berkeley National Laboratory, using synchrotron radiation ( $\lambda = 0.7749 \text{ \AA}$ ) with a Bruker PHOTON100 CMOS detector on a D8 diffractometer. The samples were cooled to a 100 K using an Oxford Cryosystems cryostream prior to data collection. Raw data were integrated and corrected for Lorentz and polarization effects using Bruker AXS SAINT<sup>[17]</sup> software and corrected for absorption using SADABS.<sup>[18]</sup> The structures were solved using intrinsic phasing methods with SHELXT<sup>[19]</sup> and refined using SHELXL<sup>[20]</sup> operated in the OLEX2 interface.<sup>[21]</sup> Thermal parameters were refined anisotropically for all non-hydrogen atoms. All framework hydrogen atoms were refined using the riding model. Hydrogen atoms on coordinated water molecules that partially occupy the framework Co sites could not be located in the electron density difference map and were omitted from the refinement but not the formula.

## 2. Results and Discussion

**Xe and Kr Adsorption Isotherms.** Single-component Xe and Kr isotherms measured for  $\text{Co}_2(m\text{-dobdc})$  and  $\text{Ni}_2(m\text{-dobdc})$  (Figure 1) indicate that Xe binds significantly more strongly to both materials than Kr, consistent with the anticipated stronger van der Waals contacts formed between the more polarizable Xe atom and the open metal coordination sites of the two frameworks. Differential heats of adsorption determined for Xe and Kr as a function of loading (Figure 2a) reveal that their binding strengths differ by approximately 8–9 kJ/mol in both frameworks, again likely a result of the large difference in their polarizabilities (4.01 vs. 2.47  $\text{m}^3$ , respectively). Furthermore, while  $\text{Co}_2(m\text{-dobdc})$  and  $\text{Ni}_2(m\text{-dobdc})$  have similar binding enthalpies for Kr, adsorption of Xe in  $\text{Ni}_2(m\text{-dobdc})$  is  $\sim 0.6$  kJ/mol more exothermic than in  $\text{Co}_2(m\text{-dobdc})$ . This result is attributed to the larger electron cloud and greater polarizability of Xe, coupled with the ability of the higher

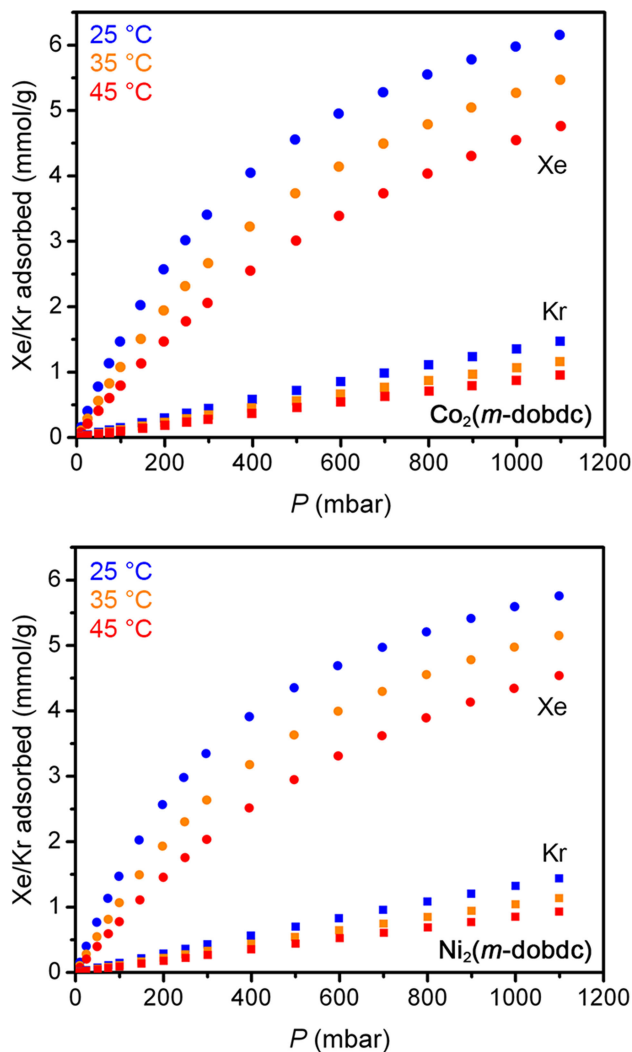


**Figure 1.** Xenon (circles) and krypton (squares) single-component adsorption isotherms for  $\text{Co}_2(m\text{-dobdc})$  (top) and  $\text{Ni}_2(m\text{-dobdc})$  (bottom) at 25 °C (blue symbols), 35 °C (orange symbols), and 45 °C (red symbols).

charge density open  $\text{Ni}^{2+}$  coordination sites to more strongly polarize the adsorbed gas.

The significant difference in Xe and Kr binding affinity at these open metal sites suggests that  $\text{Co}_2(m\text{-dobdc})$  and  $\text{Ni}_2(m\text{-dobdc})$  may be capable of separating a mixture of these gases in an adsorptive-based separation, potentially providing high selectivities while requiring significantly lower energy input than cryogenic distillation. To evaluate the potential of both frameworks in a Xe/Kr separation, we calculated selectivities for a mixture of Xe and Kr over a wide range of compositions using ideal adsorbed solution theory (IAST, Figure 2b). Notably, both materials exhibit selectivities greater than 10 for all Xe:Kr compositions (ranging from 95:5–5:95). These values are among the highest reported in the literature, comparable to  $\text{Ag}@\text{Ni}_2(\text{dobdc})$ <sup>[7d-e,9b]</sup> and are only surpassed by CaSDB (SDB<sup>2-</sup> = 4,4-sulfonyldibenzoate, also known as

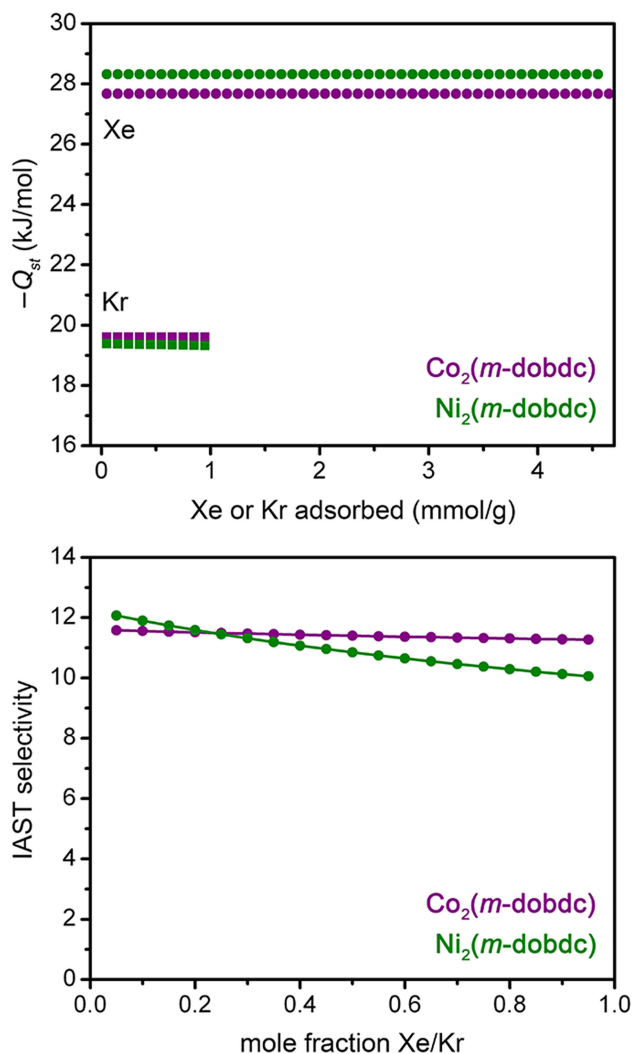


**Figure 2.** (Top) Calculated isosteric heats of adsorption calculated for Xe (circles) and Kr (squares) in  $\text{Co}_2(m\text{-dobdc})$  (purple) and  $\text{Ni}_2(m\text{-dobdc})$  (green). (Bottom) Ideal Adsorbed Solution Theory (IAST) selectivities for Xe/Kr in  $\text{Co}_2(m\text{-dobdc})$  (purple) and  $\text{Ni}_2(m\text{-dobdc})$  (green).

SB-MOF-1).<sup>[22]</sup> This material binds Xe in a very snug binding pocket, leading to strong selectivity of 16 for Xe of Kr but also slower kinetics of diffusion in and out of the material. The higher density of strong binding sites in  $M_2(m\text{-dobdc})$  and larger apertures are expected to yield higher capacities and faster diffusion of the gases through the pores, which is borne out in the Xe capacity of  $>5.5$  mmol/g in  $\text{Co}_2(m\text{-dobdc})$  and  $\text{Ni}_2(m\text{-dobdc})$  compared with only 1.4 mmol/g in CaSDB. This combination of faster diffusion, higher capacity, and high selectivity ( $\sim 11.8$  for an 80:20 Kr:Xe mixture in both  $\text{Co}_2(m\text{-dobdc})$  and  $\text{Ni}_2(m\text{-dobdc})$ ) make these materials leaders for this separation.

The selectivity values in  $M_2(m\text{-dobdc})$  are comparable to those reported for  $\text{Co}_2(\text{dobdc})$ , despite the expected stronger polarization by the  $M_2(m\text{-dobdc})$  frameworks as a result of

increased charge density at their metal sites.<sup>[14]</sup> Interestingly,  $\text{Ni}_2(m\text{-dobdc})$  exhibits a broader selectivity range than  $\text{Co}_2(m\text{-dobdc})$  over the investigated compositions, and the origin of this difference is unknown at present. Additional experiments, including multicomponent adsorption measurements, would be valuable to determine actual selectivities in a mixed-gas system.

**In Situ X-ray Diffraction Experiments.** *In situ* gas-dosing powder X-ray diffraction studies were carried out to better understand the mechanism of Xe and Kr binding in  $\text{Co}_2(m\text{-dobdc})$  and  $\text{Ni}_2(m\text{-dobdc})$ . In each framework, at 250 K a single Kr adsorption site was located directly over the open metal centers at a distance of 3.122(9) Å in  $\text{Co}_2(m\text{-dobdc})$  and 3.156(14) Å in  $\text{Ni}_2(m\text{-dobdc})$  (Figure 3a), with respective refined site occupancies of 55.0(3)% and 42.5(4)%. At 200 K, no additional electron density was found that would correspond to additional adsorption sites. A single adsorption site above the metal center was also located for Xe-loaded  $\text{Co}_2(m\text{-dobdc})$  and  $\text{Ni}_2(m\text{-dobdc})$ , although the site occupancies were substantially higher at 65.0(4)% and 72.6(2)%, respectively, at 250 K (see Figures S6-7 and Supporting Info for full details).

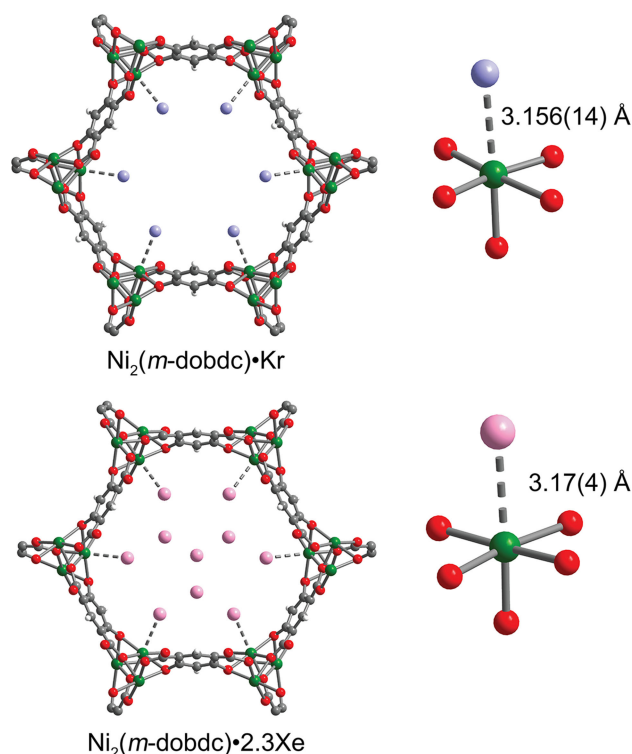


**Figure 3.** Structural models of Kr- (top) and Xe-loaded (bottom)  $\text{Ni}_2(m\text{-dobdc})$  as determined by Rietveld refinement using powder X-ray diffraction data collected at 200 K. Green, red, gray, white, purple, and pink spheres represent Ni, O, C, H, Kr, and Xe atoms, respectively.

The same Xe adsorption sites were found to increase in occupancy for both frameworks at 200 K (Co: 97.9(4)%, Ni:

96.0(9)%), and the metal-Xe interaction distances were determined to be 3.22(3) Å for  $\text{Co}_2(m\text{-dobdc})$  and 3.17(4) Å for  $\text{Ni}_2(m\text{-dobdc})$  (Figure 3b). Although these distances are longer than the measured metal-Kr distances, after accounting for differences in the van der Waals radii of the two gases, the distances indicate that the metal-Xe interaction is significantly stronger than the metal-Kr interaction. We note that a similar Co-Xe distance of 3.1772(13) Å was observed in the 100-K single-crystal X-ray diffraction structure of  $\text{Co}_2(m\text{-dobdc})(\text{H}_2\text{O})_{0.9}0.7\text{Xe}$ .

In the case of Xe, powder X-ray diffraction data revealed a second adsorption site located 4.50(7) Å (Ni, Figure 3b) and 4.42(3) Å (Co) from the primary adsorption site, and situated on a mirror plane that runs through the pore. Xenon located at the secondary site exhibits lower occupancies compared to the primary site (68.5(9)% for  $\text{Co}_2(m\text{-dobdc})$  and 42.3(14)% for  $\text{Ni}_2(m\text{-dobdc})$ ). Finally, a third xenon adsorption site was found at the center of the pore approximately 4.67 Å (Ni, Figure 3b) and 4.76 Å (Co) from the second site, with occupancies of 68.7(15)% and 54(2)% in  $\text{Co}_2(m\text{-dobdc})$  and  $\text{Ni}_2(m\text{-dobdc})$ , respectively. The higher occupancies observed for  $\text{Co}_2(m\text{-dobdc})$  relative to  $\text{Ni}_2(m\text{-dobdc})$  at all sites likely arise from the slightly higher pressure of xenon that was dosed into the  $\text{Co}_2(m\text{-dobdc})$  sample relative to  $\text{Ni}_2(m\text{-dobdc})$ . Notably, these Xe...Xe contact distances between sites are only slightly longer than those seen between xenon molecules in crystal structures of the pure gas (~4.34 Å) collected at 26 K, as well as the van der Waals diameter of xenon (4.32 Å).<sup>[23]</sup> The packing of xenon atoms within the pore channels also closely resembles the hexagonal close packing in the crystal structure of the pure gas at 26 K, with the first and third site forming a hexagonal arrangement, followed by a layer of three symmetry-equivalent secondary sites (see Supporting Information Figures S9–S10). The hexagonal space group of the frameworks likely helps template this arrangement, as all adsorption sites are either on special positions or above the open metal sites.

The significant differences between the adsorbed krypton and adsorbed xenon structures agree well with the more exothermic enthalpy of adsorption of xenon in comparison to krypton, as discussed above. Moreover, the lack of secondary and tertiary Kr binding sites at temperatures where these sites are observed for Xe indicates that Xe interactions with the frameworks and nearby Xe atoms further contribute to its stronger adsorption by  $\text{Co}_2(m\text{-dobdc})$  and  $\text{Ni}_2(m\text{-dobdc})$ . We note that the structural differences between adsorbed krypton and xenon in  $\text{Co}_2(m\text{-dobdc})$  and  $\text{Ni}_2(m\text{-dobdc})$  are similar to those observed for  $\text{M}_2(\text{dobdc})$  in previous reports.<sup>[9c,24]</sup> For example, Xe has been shown to adsorb at three unique sites in  $\text{Ni}_2(\text{dobdc})$ . However,  $\text{Co}_2(m\text{-dobdc})$  and  $\text{Ni}_2(m\text{-dobdc})$  do not show evidence for a second Kr adsorption site, unlike studies on  $\text{Ni}_2(\text{dobdc})$  obtained at lower temperatures and higher pressures.<sup>[9c,22]</sup> The distances between the metal and adsorbed gases in these previously reported structural studies are also similar to those found in this report.

### 3. Conclusions

We have shown that the metal-organic frameworks  $\text{Co}_2(m\text{-dobdc})$  and  $\text{Ni}_2(m\text{-dobdc})$  adsorb xenon with greater affinity and selectivity than krypton, consistent with the greater polarizability of Xe and the large positive charge density at the coordinatively-unsaturated metal cation sites within both frameworks. Both frameworks exhibit a negative enthalpy of adsorption for xenon that is ~8–9 kJ/mol larger in magnitude than for krypton, and, as a result, IAST selectivities greater than 10 for Xe:Kr compositions between 95:5 and 5:95 at 25 °C. *In situ* gas-dosing powder X-ray diffraction data further confirmed that xenon has a stronger interaction with the open metal sites of both materials, as evident from the larger occupancies for adsorbed xenon over the framework open metal. Strikingly, adsorbed xenon at higher occupancies also shows preferences for two additional sites within the framework channels, leading to close Xe...Xe contacts reminiscent of the crystal structure of xenon at 26 K. Such a close packing likely contributes to the high adsorption capacities observed for xenon at higher pressures in gas adsorption measurements, relative to the much lower capacities observed for krypton. Overall, these results offer an interesting comparison to previously reported studies of Xe/Kr adsorption in  $\text{M}_2(\text{dobdc})$  and suggest that  $\text{Co}_2(m\text{-dobdc})$  and  $\text{Ni}_2(m\text{-dobdc})$  may be efficient adsorbents for the separation of Xe/Kr, and therefore promising alternatives to cryogenic distillation. Further experiments are needed to evaluate the affinities and selectivities under more realistic mixed-gas conditions.

### Associated Content

**Supporting Information.** Additional framework characterization, experimental details, powder X-ray diffraction analysis details, single-crystal X-ray diffraction data, and other details are available in the supporting information. This material is available free of charge via the internet.

### Notes

The authors declare the following competing financial interests: J.R.L. has a financial interest in Mosaic Materials, Inc., a startup working to commercialize metal-organic frameworks, including the  $\text{M}_2(m\text{-dobdc})$  materials discussed herein. The University of California, Berkeley, has applied for a patent on some of the materials discussed herein, on which J.R.L. and M.T.K. are listed as inventors.

### Acknowledgements

This research was supported through the Center for Gas Separations Relevant to Clean Energy Technologies, an Energy Frontier Research Center funded by the U.S. Depart-

ment of Energy, Office of Science, Office of Basic Energy Sciences under Award DE-SC0001015. Powder X-ray diffraction data were collected on the 17-BM-B Beamline at the Advanced Photon Source, a U.S. Department of Energy Office of Science User Facility operated by Argonne National Laboratory. Use of the Advanced Photon Source at Argonne National Laboratory was supported by the U.S. Department of Energy, Office of Science, Office of Basic Energy Sciences, under Contract No. DE-AC02-06CH11357. Single-crystal X-ray diffraction data was collected at Beamline 11.3.1 of the Advanced Light Source, which is supported by the Director, Office of Science, Office of Basic Energy Sciences, of the U.S. Department of Energy under contract no. DE-AC02-05CH11231. M.T.K. and J.O. thank the NSF for graduate fellowship support. Dr. Katie R. Meihaus is thanked for editorial assistance.

## References

- [1] C. M. Simon, R. Mercado, S. K. Schnell, B. Smit, M. Haranczyk, *Chem. Mater.* **2015**, *27*, 4459–4475.
- [2] G. E. Pavlovskaya, Z. I. Cleveland, K. F. Stupic, R. J. Basaraba, T. Meersmann, *Proc. Natl. Acad. Sci. USA* **2005**, *102*, 18275–18279.
- [3] F. G. Kerry, *Industrial Gas Handbook: Gas Purification and Separation*; CRC: Boca Raton, FL, **2007**, chapter 4.4.
- [4] L. Chen, P. S. Reiss, S. Y. Chong, D. Holden, K. E. Jelfs, T. Hasell, M. A. Little, A. Kewley, M. E. Birggs, A. Stephenson, K. M. Thomas, J. A. Armstrong, J. Bell, J. Busto, R. Noel, J. Liu, D. M. Strachan, P. K. Thallapally, A. I. Cooper, *Nat. Mater.* **2014**, *13*, 954–960.
- [5] a) K. Munakata, T. Fukumatsu, S. Yamatsuki, K. Tanaka, M. Nishikawa, *J. Nucl. Sci. Technol.* **1999**, *36*, 818–829. b) R. E. Bazan, M. Bastos-Neto, A. Moeller, F. Dreisbach, R. Staudt, *Adsorption* **2011**, *17*, 371–383.
- [6] a) R. I. Derrah, D. M. Ruthven, *Can. J. Chem.* **1975**, *53*, 996–1006. b) C. J. Jameson, A. K. Jameson, H.-M. Lim, *J. Chem. Phys.* **1997**, *107*, 4364–4372.
- [7] a) C. A. Fernandez, J. Liu, P. K. Thallapally, D. M. Strachan, *J. Am. Chem. Soc.* **2012**, *134*, 9046–9049. b) Y.-S. Bae, B. G. Hauser, Y. J. Colón, J. T. Hupp, O. K. Farha, R. Q. Snurr, *Microporous Mesoporous Mater.* **2013**, *169*, 176–179. c) H. Wang, K. Yao, Z. Zhang, J. Jagiello, Q. Gong, Y. Han, J. Li, *Chem. Sci.* **2014**, *5*, 620–624. d) X. Chen, A. M. Plonka, D. Banerjee, R. Krishna, H. T. Schaef, S. Ghose, P. K. Thallapally, J. B. Parise, *J. Am. Chem. Soc.* **2015**, *137*, 7007–7010. e) D. Banerjee, A. J. Cairns, J. Liu, R. K. Motkuri, S. K. Nune, C. A. Fernandez, R. Krishna, D. M. Strachan, P. K. Thallapally, *Acc. Chem. Res.* **2015**, *48*, 211–219.
- [8] H. Bunzen, F. Kolbe, A. Kalytta-Mewes, G. Sastre, E. Brunner, D. Volkmer, *J. Am. Chem. Soc.* **2018**, DOI: 10.1021/jacs.8b04582.
- [9] a) P. K. Thallapally, J. W. Grate, R. K. Motkuri, *Chem. Commun.* **2012**, *48*, 347–349. b) J. Liu, D. M. Strachan, P. K. Thallapally, *Chem. Commun.* **2014**, *50*, 466–468. c) O. V. Magdysyuk, F. Adams, H.-P. Liermann, I. Spanopoulos, P. N. Trikalitis, M. Hirscher, R. E. Morris, M. J. Duncan, L. J. McCormick, R. E. Dinnebie, *Phys. Chem. Chem. Phys.* **2014**, *16*, 23908–23914.
- [10] a) N. L. Rosi, J. Kim, M. Eddaoudi, B. Chen, M. O’Keeffe, O. M. Yaghi, *J. Am. Chem. Soc.* **2005**, *127*, 1504; b) S. R. Caskey, A. G. Wong-Foy, A. J. Matzger, *J. Am. Chem. Soc.* **2008**, *130*, 10870; c) E. D. Bloch, L. J. Murray, W. L. Queen, S. Chavan, S. N. Maximoff, J. P. Bigi, R. Krishna, V. K. Peterson, F. Grandjean, G. J. Long, B. Smit, S. Bordiga, C. M. Brown, J. R. Long, *J. Am. Chem. Soc.* **2011**, *133*, 14814.
- [11] J. Liu, P. K. Thallapally, D. Strachan, *Langmuir*, **2012**, *28*, 11584–11589.
- [12] S.-J. Lee, K. C. Kim, T.-U. Yoon, M.-B. Kim, Y.-S. Bae, *Microporous Mesoporous Mater.* **2016**, *236*, 284–291.
- [13] T. Vazhappilly, T. K. Ghanty, B. N. Jagatap, *J. Phys. Chem. C* **2016**, *120*, 10968–10974.
- [14] M. T. Kapelewski, S. J. Geier, M. R. Hudson, D. Stück, J. A. Mason, J. N. Nelson, D. J. Xiao, Z. Hulvey, E. Gilmour, S. A. FitzGerald, M. Head-Gordon, C. M. Brown, J. R. Long, *J. Am. Chem. Soc.* **2014**, *136*, 12119–12129.
- [15] D. DeSantis, J. A. Mason, B. D. James, C. Houchins, J. R. Long, M. Veenstra, *Energy Fuels*, **2017**, *31*, 2024–2032.
- [16] J. E. Bachman, M. T. Kapelewski, D. A. Reed, M. I. Gonzalez, J. R. Long, *J. Am. Chem. Soc.* **2017**, *139*, 15363–15370.
- [17] Bruker Analytical X-ray Systems, Inc. *SAINT and APEX 2 Software for CCD Diffractometers; Bruker Analytical X-ray Systems, Inc.*: Madison, WI, 2000.
- [18] G. M. Sheldrick, *SADABS*; Bruker Analytical X-ray Systems, Inc.: Madison, WI, 2014.
- [19] G. M. Sheldrick, *Acta Crystallogr., Sect. A: Found. Adv.* **2015**, *71*, 3.
- [20] G. M. Sheldrick, *Acta Crystallogr., Sect. A: Found. Crystallogr.* **2008**, *64*, 112, b) G. M. Sheldrick, *SHELXL*; University of Göttingen: Germany, **2014**.
- [21] O. V. Dolomanov, L. J. Bourhis, R. J. Gildea, J. A. K. Howard, H. J. Puschmann, *Appl. Crystallogr.* **2009**, *42*, 339.
- [22] D. Bannerjee, C. M. Simon, A. M. Plonka, R. K. Motkuri, J. Liu, X. Chen, B. Smit, J. B. Parise, M. Haranczyk, P. K. Thallapally, *Nature Commun.* **2016**, *7*, 11831.
- [23] a) D. R. Sears, H. P. Klug, *J. Chem. Phys.* **1962**, *37*, 3002. b) Y. Sonnenblick, E. Alexander, Z. H. Kalman, I. T. Steinberger, *Chem. Phys. Lett.* **1977**, *52*, 276–278.
- [24] S. K. Ghose, Y. Li, A. Yakovenko, E. Dooryhee, L. Ehm, L. E. Ecker, A.-C. Dippel, G. J. Halder, D. M. Strachan, P. K. Thallapally, *J. Phys. Chem. Lett.* **2015**, *6*, 1790–1794.

Received: August 15, 2018

Accepted: August 18, 2018

Published online on September 11, 2018